CHEMISTRY OF MATERIALS

Article

pubs.acs.org/cm

Anisotropic Atomic Layer Deposition Profiles of TiO_2 in Hierarchical Silica Material with Multiple Porosity

Sreeprasanth Pulinthanathu Sree,[#,†] Jolien Dendooven,[#,‡] Jasper Jammaer,[†] Kasper Masschaele,[†] Davy Deduytsche,[‡] Jan D'Haen,[§] Christine E. A. Kirschhock,[†] Johan A. Martens,*[,†] and Christophe Detavernier[‡]

[†]Centre for Surface Chemistry and Catalysis, KU Leuven, Kasteelpark Arenberg 23, B-3001 Leuven, Belgium

[‡]Department of Solid State Sciences, Ghent University, Krijgslaan 281/S1, B-9000 Gent, Belgium

[§]IMO-IMOMEC, University of Hasselt, Diepenbeek, Belgium

S *Supporting Information*

ABSTRACT: Anisotropic deposition profiles of TiO_2 in Zeotile-4 ordered mesoporous silica material are obtained using Atomic Layer Deposition (ALD) involving alternating pulses of tetrakis(dimethylamino) titanium (TDMAT) and water. TiO_2 concentration profiles visualized by transmission electron microscopy (TEM) on particle cross sections reveal the systematic deeper penetration of the deposition front along the main channels and the more limited penetration in the perpendicular direction through the narrower slit-like mesopores. In ordered mesoporous material with one-dimensional pore system ALD leads to pore plugging. Diffusion limited ALD is shown to be useful for TiO_2 deposition in anisotropic mesoporous support materials.

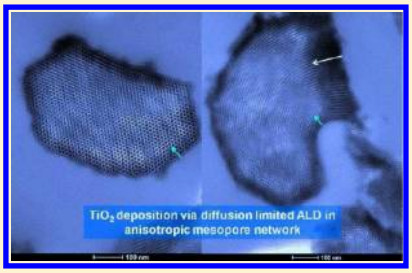

KEYWORDS: *atomic layer deposition, mesopores, zeotile-4*

I. INTRODUCTION

Atomic layer deposition (ALD) is an ultrathin coating technique relying on sequential self-terminating reactions between a vapor and a solid surface. ALD is an elegant method for modifying surfaces for application in microelectronics, fuel cells, batteries, filtration devices, sensors, and other fields, where the technique is appreciated for its excellent conformality and precision of film thickness.[1−3] ALD has been applied successfully on nanomaterials such as nanowires, nanotubes, and nanoparticles, fibrous materials, and nanosized powders[1,2,4,5] and has been introduced in the world of porous materials for tuning the pore size of nanoporous membranes,[6,7] thin films[8,9] and engineering the presence of catalytic sites on the pore walls.[10,11] Modification through ALD of silica gel having an unordered pore network consisting of 30 nm wide pores is well documented and, for example, Al_2O_3, ZnO, TiO_2, and AlN have been deposited.[12−16]

Ordered mesoporous silica materials have been around for two decades. The accessibility of the mesopores to (bio) molecules and functional nanoparticles has been demonstrated and evaluated in various applications such as, for example, drug delivery, catalysis, molecular separation, and sensors.[17−21] The incorporation of active elements in pore walls of ordered mesoporous silica materials has been achieved during synthesis or through post-synthesis modification via impregnation, grafting, and chemical vapor infiltration.[22] TiO_2 grafted on ordered mesoporous silica serves as photocatalyst for elimination of air and water borne pollutants.[23] Also the incorporation of titania into silicate zeolites to generate photocatalytic activity is well documented.[24] While the synthesis of P6m ordered mesoporous silica by now is easy,[25] uniform coating of the pore walls with an inorganic film is not straightforward. Recently, some papers reported the use of ALD for tailoring the surface of ordered mesoporous materials. Hukkamäki et al. introduced cobalt into MCM-41 and SBA-15 samples with pore diameters of 2.8 and 5.6 nm, respectively, using 3 consecutive depositions of $Co_2(CO)_8$ precursor for 6 h at 50 °C and intermittent carbonylation at 150 °C.[26] The observation of a decrease of pore volume at constant pore size was interpreted as a blocking of pore entrances. Muylaert et al. deposited a small amount of TiO_2 and VOx on the surface of SBA-15 with a pore size of 6.5 nm, using tetrakis-(dimethylamino)titanium (TDMAT) and vanadyl isopropoxide as precursors.[27] The metal loading was varied by the exposure time of the precursors and was found to have a significant impact on the selectivity of the synthesized catalysts in the liquid phase epoxidation of cyclohexene. Pagán-Torres et al. performed ALD of Nb_2O_5 on SBA-15 powder having 6.5 nm wide pores. The ALD process was performed at 135 °C and involved alternating exposure to niobium ethoxide and water in 14 min cycles.[28] Interestingly, the first niobia depositions filled up the micropores contained in the mesopore walls. At high Nb_2O_5 loading of 32%, the microporosity was eliminated and the free diameter of the mesopores systematically was reduced from the initial 6.5 to 3.7 nm. The free pore volume was

Received: April 19, 2012
Revised: June 11, 2012
Published: June 20, 2012

   dx.doi.org/10.1021/cm301205p | *Chem. Mater.* 2012, 24, 2775−2780

decreased from 1.1 to 0.14 cm^3/g. Evidence for uniform coating of the mesopore walls was obtained from STEM.

In this work, we performed ALD of TiO_2 into Zeotile-4, a three-dimensional (3D) ordered mesoporous silica material with 2 types of mesopores as well as micropores.[29−32] By varying the Ti-precursor exposure time, we investigated the introduction of TiO_2 into the differently sized pores of Zeotile-4. The deposition was aimed at exploring the potential of ALD in functionalizing the internal porosity of a mesoporous material without creating pore-plugging. For comparison, similar ALD treatments were performed on COK-12, an ordered mesoporous silica material containing hexagonally ordered one-dimensional (1D) mesopores.[25]

II. EXPERIMENTAL PROCEDURES

Synthesis of Mesoporous Powders. Zeotile-4 material is prepared by adapting the synthesis procedure reported in ref 31. This involves the preparation of a clear solution of silica nanoslabs (silicalite precursors) and combining it with Pluronic 123 followed by aging them at high temperature. For preparing the clear solution first TEOS is mixed with TPAOH under vigorous stirring facilitating the hydrolysis of TEOS. Then water is added to the suspension and kept on stirring for another 24 h. The TEOS: TPAOH: H_2O molar ratio was maintained to be 25: 9: 400. Then 18 g of this clear solution was added to 9 g of HCl (5M) and is mixed with 24 g of aqueous Pluronic P123 solution (10 wt %) which has been already acidified using 8 g of 5 M HCl. The mixture is kept at 95 °C for 96 h, and then the solid precipitate formed is washed, dried, and calcined at 350 °C for 12 h using slow heating ramp of 0.5 °C/min.

COK-12 materials were prepared based on a procedure reported by Jammaer et al.[25] Approximately 10 g of material was produced by first disolving 14.6 g of pluronic P123 in a buffer consisting of 13.1 g of citric acid (monohydrate), 9.0 g of trisodium citrate (dehydrate), and 382.2 g of H_2O. A sodium silicate solution is prepared by diluting 37.0 g of sodium silicate solution with 106.9 g of H_2O. The latter is added in a swift movement to the surfactant solution, and the product slurry is kept overnight at room temperature. Subsequently the slurry is vacuum filtered and washed abundantly with water. Drying was performed at 60 °C and calcination was performed at 500 °C for 6 h using a 1 °C/min ramp.

TiO_2 ALD on to Mesoporous Powders. Five samples, that is, TiO_2 coated Zeotile-4 or COK-12 powder, were synthesized via ALD (Table 1). In each case, about 100 mg of powder was placed in an aluminum boat and loaded into a pump-type ALD chamber trough a loadlock. The loadlock was slowly pumped through a needle valve to prevent loss of the powders. The ALD chamber was pumped by a turbomolecular pump, resulting in a base pressure of about 10^{-6} mbar. Prior to the deposition, the powders were outgassed by keeping them at elevated temperature for a few hours. TiO_2 was deposited from tetrakis(dimethylamino)titanium (TDMAT) and H_2O. The TDMAT stainless steel container was heated to 45 °C, the H_2O container was kept at room temperature, and both gas lines were heated to 50 °C to prevent condensation. All samples were exposed to 30 ALD cycles. The exposure times are indicated in Table 1. During the TDMAT exposures, argon was used as a carrier gas, and the pressure in the ALD chamber was about 0.15 Pa. Without argon carrier gas flowing, the TDMAT pressure measured in the ALD chamber was in the range 0.008−0.02 Pa. During the water exposures, the pressure was about 0.15 Pa. The deposition temperature for sample 1 and 2 (30 s and 90 s pulses) was 200 °C but for samples prepared at longer exposures (150 s and 300 s) the temperature was kept at 120 °C to avoid the decomposition of the TDMAT precursor in the gas phase.[33,34]

Table 1. ALD Conditions for TiO_2 Introduction into Zeotile-4 and COK-12 Powders[a]

sample	ALD temperature (°C)	TDMAT exposure time per cycle[b] (s)	TiO_2 (mol %)[c]
Zeotile-4 (30s)	200	30	N.D.[d]
Zeotile-4 (90s)	200	90	N.D.[d]
Zeotile-4 (150s)	120	150	5
Zeotile-4 (300s)	120	300	12
COK-12 (300s)	120	300	7

[a]30 ALD cycles on each sample. [b]The water exposure time was set equal to the TDMAT exposure time; the evacuation times were set to twice the value of TDMAT exposure time. [c]Determined by XRF. [d]Not determined.

Characterization. For preparing the specimens for Transmission Electron Microscopy (TEM) measurements, ALD treated Zeotile-4 powder was first embedded in a Struers SpeciFix-20 resin. Then electron transparent thin slices of about 100 nm were prepared using a Leica EMFCS ultra microtome. The cut samples were investigated with a FEI Tecnai Spirit scanning transmission electron microscope (TEM). TEM bright field (BF) images are recorded with a 4k × 4k Eagle CCD camera. High angle annular dark field scanning transmission electron microscope (HAADF STEM) images are also recorded. X-ray fluorescence (XRF) measurements were performed using a Bruker Artax system consisting of a Mo X-ray source and an XFlash 5010 silicon drift detector. N_2 physisorption measurements were performed on a Quantachrome Autosorb-1. The samples were pretreated at 100 °C under vacuum for 12 h. Small Angle X-ray Scattering (SAXS) on powder samples were done on SAXSess mc^2 Anton Paar apparatus. Powders were loaded in plastic capillaries and the patterns were corrected for background.

III. RESULTS AND DISCUSSION

Zeotile-4 has a 3D mosaic structure obtained by tiling rectangular 4 × 8 × 2 nm^3 nanoslabs according to a hexagonal pattern.[31,32] The nanoslabs themselves have emerging zeolitic character and provide internal microporosity. Successive layers composed of nanoslabs are rotated by 120° resulting in a 3D mesoporosity with parallel main channels interconnected at regular distances by slits between stapled nanoslabs (Figure1).

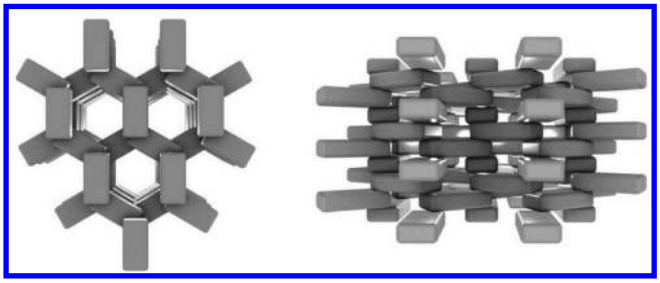

Figure 1. Tiling pattern of nanoslabs in Zeotile-4 material. Left; view along the main mesopores (pore size ca. 10 nm), right; sideways view on the slit-like pores (pore size between 2−4 nm).

Zeotile-4 is synthesized using a dual template approach with tetrapropylammonium template for creating micropores and triblock copolymer Pluronic P123 surfactant for obtaining the specific mesostructuring.[31,32] The unique hierarchical structure of Zeotile-4 and its tiling of nanoslab building units have been revealed using discrete tomography.[31]

ALD of TiO_2 on Zeotile-4 powder was performed using TDMAT and water.[35] This process is known to result in amorphous TiO_2 coatings.[35,36] The conditions used for ALD on the different samples are listed in Table 1. In the first experiments using 30 and 90 s TDMAT exposure times, the deposition temperature was 200 °C. For longer TDMAT

dx.doi.org/10.1021/cm301205p | Chem. Mater. 2012, 24, 2775−2780

exposure times of 150 and 300 s, it was necessary to reduce the deposition temperature to 120 °C to avoid substantial decomposition of the Ti-precursor. During the TDMAT (with argon carrier gas flowing) and water exposures, the pressure in the ALD chamber was about 0.15 Pa. On all the samples 30 ALD cycles were performed.

XRF measurements on the ALD treated Zeotile-4 samples showed a maximum TiO_2 loading of 12 mol-% TiO_2 for the sample exposed to 30 ALD cycles using 300 s TDMAT exposure time (Table 1). SAXS patterns of the parent and ALD treated Zeotile-4 samples revealed that the material retained its structure (Supporting Information). The unit cell parameters of the parent and treated samples were similar (~14 nm).

The infiltration of TiO_2 into the Zeotile-4 samples was investigated using TEM. After ALD, the powders were embedded in a Struers Specifix-20 resin, and about 100 nm thin slices were prepared using an ultramicrotome. A TEM image of Zeotile-4(90s) at low magnification is shown in Figure 2.

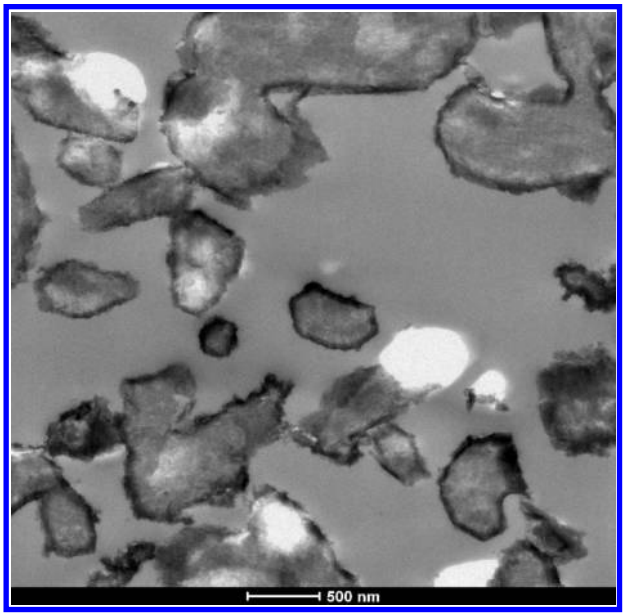

Figure 2. TEM on Zeotile-4 (90s) at a lower magnification indicating the uniformity of TiO_2 deposition (dark rims) on the individual powder particles.

The enrichment of Ti in the rim of the particles was revealed by a contrast difference due to the increased electron absorption, which the parent Zeotile-4 sample did not show. Energy dispersive X-ray (EDX) measurements on Zeotile-4 particles confirmed the presence of Ti, whereas EDX on the resin areas between the particles showed absence of Ti and Si (Supporting Information). The uniformity of Ti introduction in different particles of a powder batch can be appreciated in the TEM image in Figure 2, showing all particles had a dark rim ascribed to the presence of TiO_2. The bright spots correspond to holes in the investigated thin slice.

TEM images of Zeotile-4 particles subjected to ALD treatments using different TDMAT exposure times are shown in Figure 3. Specimens with orientation in the direction of the main channel of the Zeotile-4 structure were selected. The dark contrast ascribed to TiO_2 coating became broader with longer TDMAT pulses. Using a 30 s TDMAT pulse in Zeotile-4(30s) (Figure 3 a, b), the dark layer measured about 20 nm. Using 90 s pulses it was extended to about 45 nm (Figure 3 c, d) while 300 s of exposure (Figure 3 e, f) resulted in a about 125 nm broad dark layer. The uniform penetration of TiO_2 in all directions perpendicular to the direction of the main channel can be understood based on the availability of slit shape mesopores allowing TDMAT to penetrate (Figure 1).

Figure 4 presents a high angle annular dark field scanning transmission electron microscope (HAADF-STEM) image in which the contrast can be directly related to the atomic number. HAADF-STEM confirmed the presence of more TiO_2 in the outer rim and gave direct evidence for progressive TiO_2 deposition toward the interior of the Zeotile-4 particles (Figure 4a). The presence of a deposition front progressing with pulse length indicated ALD under the applied conditions was diffusion limited. The diffusion of TDMAT precursors can occur both through the main straight channels, the slit shape narrower mesopores, and the micropores inside the nanoslabs. Occasionally, we encountered a Zeotile-4(90s) particle that was cut parallel to the main channels (Figure 5). In the direction of the main pores (white arrow) the dark area corresponding to TiO_2 deposition was about 150 nm, while in perpendicular directions (green arrows) penetration was limited to about 50 nm due to ALD through narrower mesopores. An earlier investigation in literature reported the diffusion limited nature of the Al_2O_3 ALD process from trimethylaluminum (TMA) and water in spherical silica gel particles.[12] Using cross sectional SEM combined with EDX, the cited authors visualized an isotropic deposition front penetrating to the core of the unordered silica gel particles. Here, TEM allowed us to reveal the anisotropic penetration of TiO_2 in ordered Zeotile-4 material.

The evolution of the porosity and surface area was probed using N_2 physisorption (Figure 6 and Table 2). The N_2 adsorption isotherm is characterized by strong N_2 uptakes at low relative pressure, ascribed to micropore filling, and a significant upswing of the isotherm and hysteresis at higher relative pressure, owing to adsorption and capillary condensation in mesopores.

The hysteresis loop with steep almost vertical branches is characteristic for a material with uniform cylindrical mesopores. The ALD treatment did not alter the shape of the isotherm but decreased the adsorbed quantity. The N_2 adsorption isotherms were analyzed using Brunauer–Emmett–Teller (BET), t-plot, and Non-Local Density Functional Theory (NLDFT)[37] methods. The parent Zeotile-4 sample had a BET surface area of 1224 m^2/g. It decreased to 829 m^2/g and 606 m^2/g after TiO_2 ALD using 30 s and 300 s TDMAT pulses, respectively. Regardless to the cycle duration, the original micropore volume of 0.11 mL/g had disappeared after ALD. The mesopore size distribution is shown in Figure 6b. Zeotile-4 presents a main type of mesopores with diameter of about 9.5 nm and a shoulder at 12 nm, next to smaller mesopores with pore widths between 2 and 8 nm. This broad pore size distribution is caused by the complicated pore architecture, in which large hexagonal channels are connected by smaller slit-like openings (Figure 1). The occurrence of some pores with apparent diameter of 12 nm can be caused by occasional stacking faults and local structural imperfections, leading to larger openings between main channels. The pore size distribution was computed assuming a cylindrical pore model.[33] Given the irregular shape, the slits could be partially included in the volume of the main channel giving rise to an artificial increase of pore size and the observed shoulder.

dx.doi.org/10.1021/cm301205p | *Chem. Mater.* 2012, 24, 2775–2780

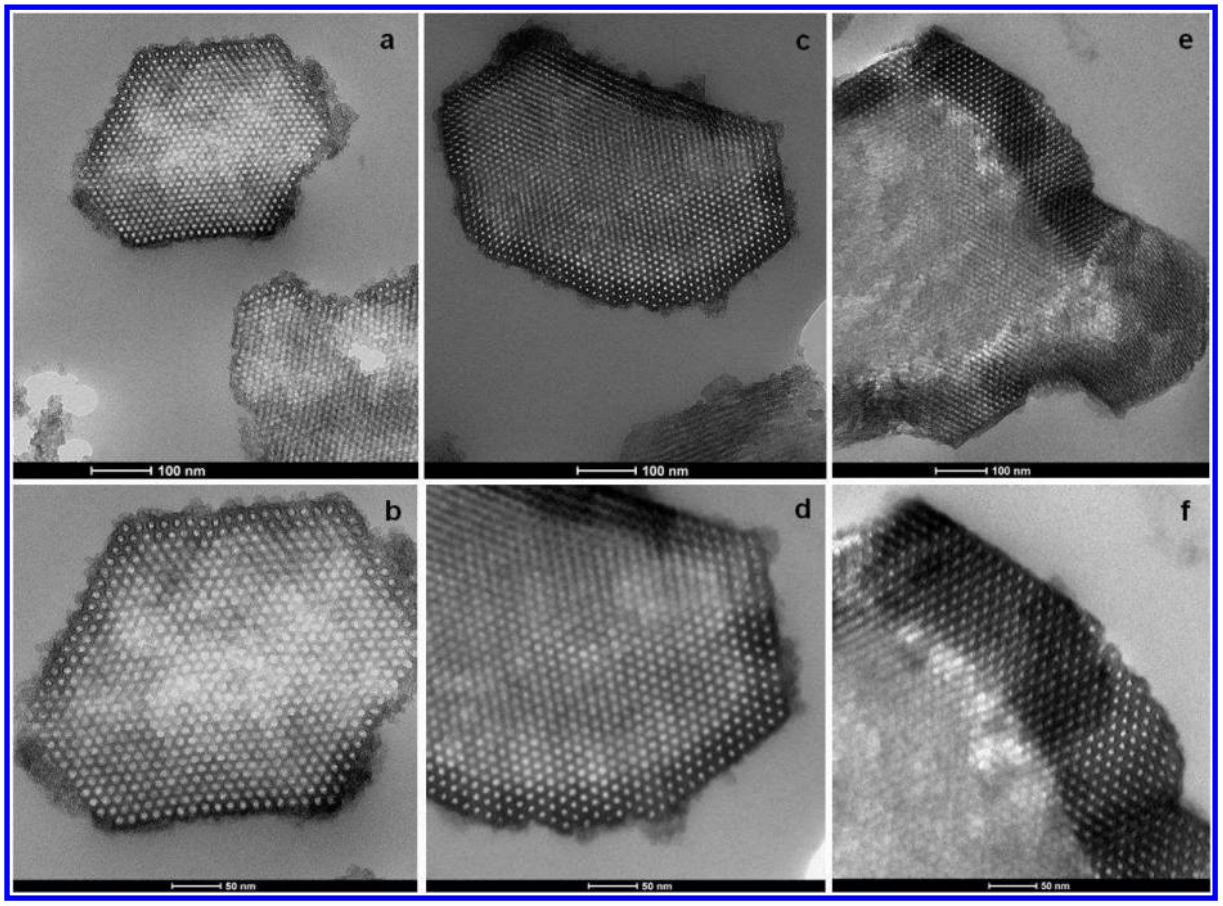

Figure 3. TEM images of TiO2-ALD modified Zeotile-4 samples at two magnifications. (a, b) Zeotile-4(30s); (c, d) Zeotile-4(90s), and (e, f) Zeotile-4(300s).

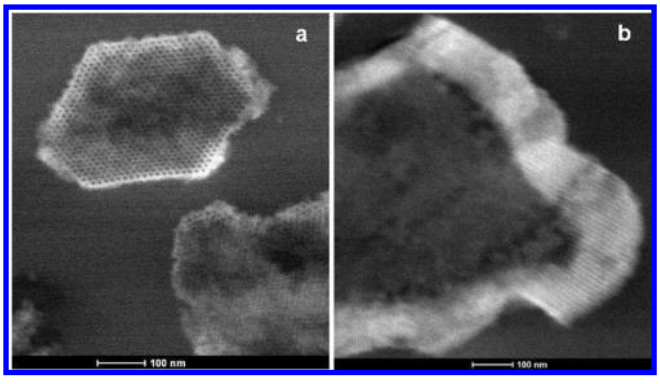

Figure 4. HAADF STEM (a) Zeotile-4(30s) and (b) Zeotile-4 (300s).

The mesopores were classified according to diameters smaller and larger than 8.5 nm (Table 2), corresponding to a division between the slit pores and the main channels (Figure 1). In the parent Zeotile-4 the volume of small mesopores and large mesopores was about 0.49 mL/g and 1.2 mL/g, respectively. In Zeotile-4(30s) sample, the volume of small mesopores was reduced to 0.32 mL/g, while there was only a minor volume reduction of the large mesopores to 1.1 mL/g. Longer TDMAT exposure on the Zeotile-4(300s) sample led to a further reduction of the volume of small mesopores to 0.22 mL/g and of the large mesopores to 0.9 mL/g. The mesopore size distribution (Figure 6b) revealed a marked evolution of the small mesopores with TiO_2 loading. The TiO_2 introduction systematically eliminated the smallest mesopores. After ALD,

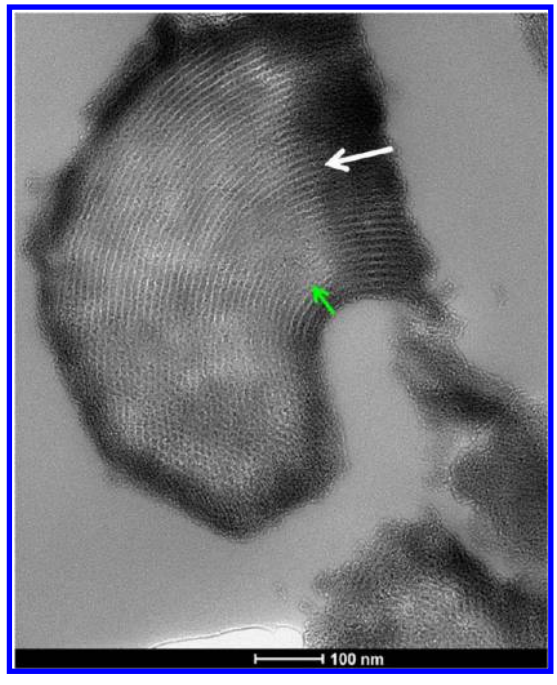

Figure 5. TEM on Zeotile-4 (90s) revealing TiO_2 infiltration in the direction of the main mesopores (white arrow) and the slits (green arrow).

the N_2 adsorption on Zeotile-4(30s) sample suggested more pores with diameters of about 12 nm were formed. Possibly,

dx.doi.org/10.1021/cm301205p | *Chem. Mater.* 2012, 24, 2775−2780

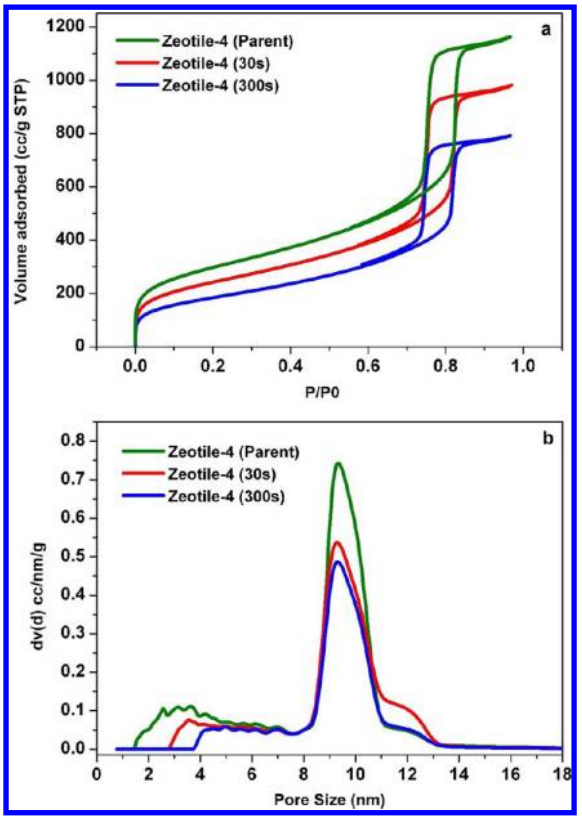

Figure 6. (a) Nitrogen adsorption isotherms and (b) pore size distributions obtained by DFT calculation using the NLDFT Equilibrium Model for the parent and TiO_2-ALD treated Zeotile-4 samples.

Table 2. Structural Properties of Parent and ALD Modified Zeotile-4 and COK-12 Powder Samples

sample name	BET SA (m^2/g)	V_{meso} (mL/g) D < 8.5 nm	V_{meso} (mL/g) D > 8.5 nm	V_{micro} (mL/g)
Zeotile-4 (Parent)	1224	0.5	1.2	0.11
Zeotile-4 (30s)	829	0.3	1.1	0.00
Zeotile-4 (300s)	606	0.2	0.9	0.00
COK-12 (Parent)	544	0.55[a]		0.08
COK-12 (300s)	474	0.47[a]		0.06

[a]Only one type of mesopores.

repeated exposure to high vacuum and humidity led to a slight increase of the already present structure defects.

The wall of the main channels presents only the small sides of the nanoblocks offering a little surface for TDMAT deposition. Surface area is mainly exposed in the slit shape mesopores, which could explain the more pronounced effect of ALD treatment on those smaller mesopores as observed in the N_2 adsorption measurements. The presence of sideways access via slit-like small mesopores is a unique feature of the Zeotile-4 material.

For comparison, the 300s deposition procedure was also applied to COK-12 powder with 1D mesoporosity. TEM images of cross sections perpendicular to the direction of the main channel (Figure 7) did not show the development of a penetration front, which is consistent with the absence of mesopores in the perpendicular directions. The shallow (<10 nm) dark rim around COK-12 particles can be due to deposition of TiO_2 on the external surface. Compared to Zeotile-4(300s), the introduced amount of Ti in COK-12(300s) was significantly lower, namely, 12 mol % TiO_2 compared to 7 mol % TiO_2 (Table 1). The lower dimensionality of the pore system may be the reason.

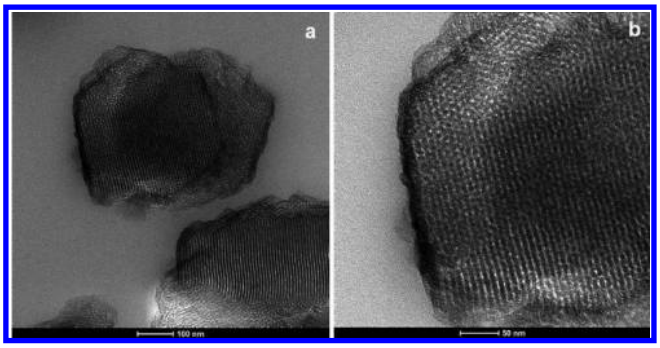

Figure 7. TEM on COK-12(300s) powder sample.

The N_2 physisorption isotherm (Figure 8) of COK-12 before and after TiO_2 ALD revealed a decrease of adsorption capacity. After ALD, the hysteresis loop extended to lower relative pressure, with is indicative of the presence of constrictions.[38]

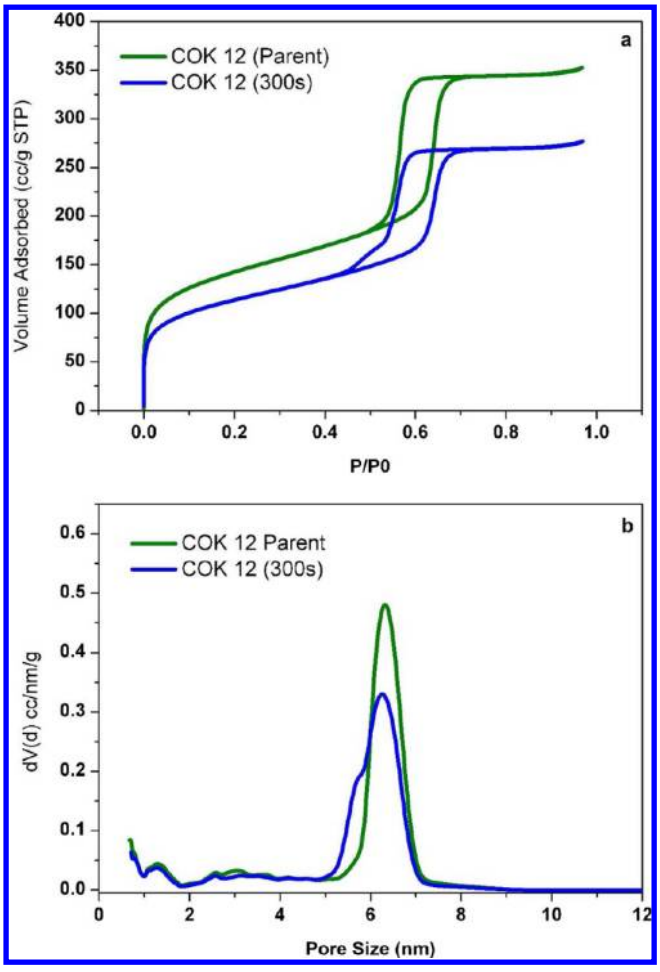

Figure 8. (a) Nitrogen adsorption isotherms and (b) pore size distributions obtained by DFT calculation using the NLDFT Equilibrium Model for the parent and TiO_2-ALD treated COK-12 (300s) sample.

dx.doi.org/10.1021/cm301205p | *Chem. Mater.* 2012, 24, 2775−2780

The narrowing of only part of the mesopores is obvious from the pore size distribution (Figure 8b). This could indicate that the TDMAT did not penetrate deep enough into the COK-12 particles to reach all potential adsorption sites.

IV. CONCLUSIONS

In conclusion, a TEM study revealed the diffusion limited nature of the TiO_2 ALD process in ordered mesoporous Zeotile-4 material. The penetration depth of the TiO_2 coating was anisotropic within this material, which could be understood based on the pore structure of the Zeotile-4 material. TiO_2 ALD can thus be used to create mesoporous materials with different penetration profiles depending on the mesopore architecture. ALD is a means to modify porosity and to introduce TiO_2 coating in the outer layers of Zeolite-4 without pore blocking. Such materials are expected to offer advantages in applications such as photocatalysis, polyfunctional catalysis, and in the development of gas sensors.

■ ASSOCIATED CONTENT

Supporting Information

SAXS patterns of parent and TiO2 deposited Zeotile-4 samples, EDX on Zeotile-4 (90 s) and on resin indicated in Figure2. This material is available free of charge via the Internet at http://pubs.acs.org.

■ AUTHOR INFORMATION

Corresponding Author

*E mail: Johan.Martens@biw.kuleuven.be.

Author Contributions

#These authors contributed equally.

Notes

The authors declare no competing financial interest.

■ ACKNOWLEDGMENTS

This work was supported by the Flemish IWT in the frame of the strategic basic research (SBO) project and by the Flemish FWO. J.A.M. acknowledges the Flemish government for long term structural funding. C.D. acknowledges the European Research Council for an ERC Starting Grant (Grant 239865), and J.D. acknowledges the Flemish FWO for a Ph.D. research grant.

■ REFERENCES

(1) Elam, J. W.; Dasgupta, N. P.; Prinz, F. B. *MRS Bull.* **2011**, *36*, 899.
(2) Marichy, C.; Bechelany, M.; Pinna, N. *Adv. Mater.* **2012**, *24*, 1017.
(3) George, S. M. *Chem. Rev.* **2010**, *110*, 111.
(4) Knez, M.; Nielsch, K.; Niinistö, L. *Adv. Mater.* **2007**, *19*, 3425.
(5) Bae, C.; Shin, H.; Nielsch, K. *MRS Bull.* **2011**, *36*, 877.
(6) Ott, A. W.; Klaus, J. W.; Johnson, J. M.; George, S. M. *Chem. Mater.* **1997**, *9*, 707.
(7) Velleman, L.; Triani, G.; Evans, J. P.; Shapter, J. G.; Losic, D. *Microporous Mesoporous Mater.* **2009**, *126*, 87.
(8) Dendooven, J.; Sree, S. P.; De Keyser, K.; Deduytsche, D.; Martens, J. A.; Ludwig, K. F.; Detavernier, C. *J. Phys. Chem. C* **2011**, *115*, 6605.
(9) Sree, S. P.; Dendooven, J.; Smeets, D.; Deduytsche, D.; Aerts, A.; Vanstreels, K.; Baklanov, M. R.; Seo, J. W.; Temst, K.; Vantomme, A.; Detavernier, C.; Martens, J. A. *J. Mater. Chem.* **2011**, *21*, 7692.
(10) Detavernier, C.; Dendooven, J.; Sree, S. P.; Ludwig, K. F.; Martens, J. A. *Chem. Soc. Rev.* **2011**, *40*, 5242.
(11) Sree, S. P.; Dendooven, J.; Koranyi, T. I.; Vanbutsele, G.; Houthoofd, K.; Deduytsche, D.; Detavernier, C.; Martens, J. A. *Catal. Sci. Technol.* **2011**, *1*, 218.
(12) Elam, J. W.; Libera, J. A.; Huynh, T. H.; Feng, H.; Pellin, M. J. *J. Phys. Chem. C* **2010**, *114*, 17286.
(13) Libera, J. A.; Elam, J. W.; Pellin, M. J. *Thin Solid Films* **2008**, *516*, 6158.
(14) Kucheyev, S. O.; Biener, J.; Wang, Y. M.; Baumann, T. F.; Wu, K. J.; van Buuren, T.; Hamza, A. V., Jr.; Satcher, J. H. *Appl. Phys. Lett.* **2005**, *86*, 083108.
(15) Lu, J.; Kosuda, K. M.; Van Duyne, R. P.; Stair, P. C. *J. Phys. Chem. C* **2009**, *113*, 12412.
(16) Pururunen, R. L.; Root, A.; Sarv, P.; Haukka, S.; Iiskola, E. I.; Lindblad, M.; Krause, A. O. I. *Appl. Surf. Sci.* **2000**, *165*, 193.
(17) Tian, R.; Zhang, H.; Ye, M.; Jiang, X.; Hu, L.; Li, X.; Bao, X.; Zou, H. *Angew. Chem., Int. Ed.* **2007**, *46*, 962.
(18) Mellaerts, R.; Aerts, C.; Van Humbeeck, J.; Augustijns, P.; Van den Mooter, G.; Martens, J. *Chem. Commun.* **2007**, *13*, 1375.
(19) Vallet-Regi, M.; Balas, F.; Arcos, D. *Angew. Chem., Int. Ed.* **2007**, *46*, 7548.
(20) Corma, A. *Chem. Rev.* **1997**, *97*, 2373.
(21) Descalzo, A. B.; Rurack, K.; Weisshoff, H.; Martınez-Manez, R.; Marcos, M. D.; Amoro, P.; Hoffmann, K.; Soto, J. *J. Am. Chem. Soc.* **2005**, *127*, 184.
(22) Linares, N.; Serrano, E.; Rico, M.; Balu, A. M.; Losada, E.; Luque, R.; Martinez, J. G. *Chem. Commun.* **2011**, *47*, 9024.
(23) Koodali, R. T.; Zhao, D. *Energy Environ. Sci.* **2010**, *3*, 608.
(24) Corma, A.; Garcia, H. *Chem. Commun.* **2004**, 1443.
(25) Jammaer, J.; van Erp, T. S.; Aerts, A.; Kirschhock, C. E. A.; Martens, J. A. *J. Am. Chem. Soc.* **2011**, *133*, 13737.
(26) Hukkamaki, J.; Suvanto, S.; Suvanto, M.; Pakkanen, T. T. *Langmuir* **2004**, *20*, 10288.
(27) Muylaert, I.; Musschoot, J.; Leus, K.; Dendooven, J.; Detavernier, C.; Van Der Voort, P. *Eur. J. Inorg. Chem.* **2012**, 251.
(28) Pagan-Torres, Y. J.; Gallo, J. M. R.; Wang, D.; Pham, H. N.; Libera, J. A.; Marshall, C. L.; Elam, J. W.; Datye, A. K.; Dumesic, J. A. *ACS Catal.* **2011**, *1*, 1234.
(29) Martens, J. A.; et al. *Catal. Today* **2011**, *168*, 17.
(30) Kirschhock, C. E. A.; Kremer, S. P. B.; Vermant, J.; Van Tendeloo, G.; Jacobs, P. A.; Martens, J. A. *Chem.—Eur. J.* **2005**, *11*, 4306.
(31) Bals, S.; Joost Batenburg, K.; Liang, D.; Lebedev, O.; Van Tendeloo, G.; Aerts, A.; Martens, J. A.; Kirschhock, C. E. A. *J. Am. Chem. Soc.* **2009**, *131*, 4771.
(32) Kremer, S. P. B.; Kirschhock, C. E. A.; Aerts, A.; Villani, K.; Martens, J. A.; Lebedev, O. I.; Van Tendeloo, G. *Adv. Mater.* **2003**, *15*, 1705.
(33) Elam, J. W.; Schuisky, M.; Ferguson, J. D.; George, S. M. *Thin Solid Films* **2003**, *436*, 145.
(34) Maeng, W. J.; Kim, H. *Electrochem. Solid-State Lett.* **2006**, *9*, G191.
(35) Xie, Q.; Jiang, Y. L.; Detavernier, C.; Deduytsche, D.; Van Meirhaeghe, R. L.; Ru, G. P.; Li, B. Z.; Qu, X. P. *J. Appl. Phys.* **2007**, *102*, 083521.
(36) Xie, Q.; Musschoot, J.; Deduytsche, D.; Van Meirhaeghe, R. L.; Detavernier, C.; Van den Berghe, S.; Jiang, Y.-L.; Ru, G.-P.; Li, B.-Z.; Qu, X.-P. *J. Electrochem. Soc.* **2008**, *155*, H688.
(37) Ravikovitch, P. I.; Neimark, A. V. *J. Phys. Chem. B* **2001**, *105*, 6817.
(38) Meynen, V.; Segura, Y.; Mertens, M.; Cool, P.; Vansant, E. F. *Microporous Mesoporous Mater.* **2005**, *85*, 119.